

Rupture characteristics of the A.D. 1912 Mürefte (Ganos) earthquake segment of the North Anatolian fault (western Turkey)

Murat Ersen Aksoy^{1,2}, Mustapha Meghraoui¹, Martin Vallée³, and Ziyadin Çakır⁴

¹Institut de Physique du Globe (UMR 7516) Strasbourg, 5 rue René Descartes, 67084 Strasbourg Cedex, France

²Eurasia Institute of Earth Sciences, Istanbul Technical University, Istanbul, Turkey

³Géoazur, Observatoire de la Côte d'Azur, IRD, Université de Nice-Sophia Antipolis, CNRS, Valbonne, France

⁴Department of Geological Engineering, Istanbul Technical University, Istanbul, Turkey

ABSTRACT

The Ganos fault is the westernmost segment of the North Anatolian fault that generated the 9 August 1912 Mürefte (Ganos) earthquake in western Turkey ($M_w = 7.4$). We study the 1912 earthquake characteristics using coseismic fault slip and fault segmentation coupled with an analysis of historical seismic records. Surface ruptures with small releasing and restraining structures and 1.5–5.5 m right-lateral offsets have been measured at 45 sites of the on-land ~45-km-long fault section. Similar structures are delineated by fresh fault scarps and prominent pull-apart basins in the Sea of Marmara and Saros Bay. A second shock with $M_w = 6.8$ occurred on 13 September 1912, implying a 20–40-km-long rupture; the damage distribution and analysis of seismic records suggest an epicenter located farther west near Saros Bay, near the western termination of the 9 August rupture. Modeling of seismic records reveals a relative source time function between the two events and indicates 40 s rupture duration, in agreement with a 120 ± 30 km-long fault rupture for the 9 August shock. An estimated 150 ± 30 km-long rupture for the two earthquakes, combined with onshore and offshore fault segmentation, allow us to better constrain the western limit of the Marmara Sea seismic gap and the related potential for a large earthquake (sharply increased by the devastating 1999 Izmit [Sea of Marmara] seismic event).

INTRODUCTION

The North Anatolian fault is a major (~1500 km long) continental strike-slip fault characterized by large earthquake ruptures (Fig. 1; Barka and Kadinsky-Cade, 1988). The North Anatolian fault in the Sea of Marmara region (western Turkey) underwent the 1912 Mürefte earthquake ($M_s 7.3 \pm 0.35$; Ambraseys and Jackson, 2000) and the 1999 Izmit earthquake ($M_w 7.4$; Barka et al., 2002) at the western and eastern ends of the Sea of Marmara, respectively (Fig. 1). At least 250 km of the North Anatolian fault might have ruptured during these 2 events, leaving a 70–150-km-long seismic gap in the Sea of Marmara (Ambraseys and Finkel, 1987; Barka et al., 2002). This large uncertainty is mostly due to the poorly known eastern extension of the 1912 earthquake rupture in the Sea of Marmara. Previous studies of the 1912 earthquake suggest 56–160 km of rupture length (Ambraseys and Jackson, 2000; Altınok et al., 2003; Le Pichon et al., 2003; Altunel et al., 2004; Armijo et al., 2005; Karabulut et al., 2006) leaving the eastern end of rupture as a matter of debate. Therefore, a better constraint of the 1912 fault rupture termination and related seismic characteristics is critical for seismic hazard assessments in Istanbul and surrounding regions (Hubert-Ferrari et al., 2000).

We present here the 1912 earthquake fault geometry and slip distribution based on aerial photographs, satellite imagery, digital elevation models, bathymetry, and field measurements.

We combine on-land investigations with the offshore fault section mapped in previous studies. The detailed fault geometry and related 1912 slip distribution on land provide hints for the fault extension offshore. The analog seismic

records allow us to deduce a focal mechanism solution and a rupture duration model. The total fault length, related geometrical complexities, and seismic characteristics are discussed to determine the Sea of Marmara seismic gap.

GANOS FAULT SEGMENT

The ENE-WSW-trending Ganos fault is a rupture segment at the westernmost section of the North Anatolian fault before it enters the North Aegean Trough of the Gulf of Saros (Fig. 1). The on-land fault appears along a narrow linear valley and forms geomorphic structures typical of strike-slip faults (releasing or restraining bends and stepovers). Figure 2 shows the fault between Gaziköy and Saros mainly delineated through stream offsets with cumulative slip varying from 10 to 600 m. The fault segment extends offshore where recent high-resolution bathymetric data and multi-channel seismic data show clear fresh fault scarps in the Sea of Marmara and in the Aegean Sea (Armijo et al., 2005; Ustaömer et al., 2008).

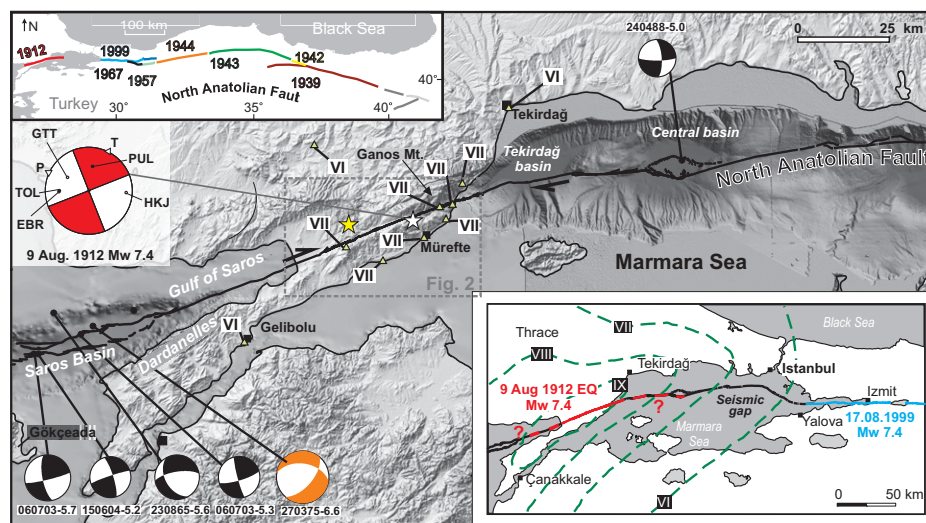


Figure 1. Seismotectonics of western Marmara region. Focal mechanisms are from Harvard Centroid Moment Tensor catalog (<http://www.globalcmt.org/>; date as day-month-year [e.g., 060703] and M_w indicated at bottom), and A.D. 1912 solution is obtained from P-wave first motions at stations PUL, GTT, EBR, TOL, and HKJ. Offshore fault trace (black lines) is modified from Armijo et al. (2005) and Ustaömer et al. (2008). White and yellow stars are 9 August and 13 September 1912 epicenters, respectively ($\pm 0.1^\circ$; Ambraseys and Jackson, 2000). Roman numerals indicate MSK (maximum intensity in Medvedev-Sponheuer-Karnik scale) intensities of 13 September event (Hecker, 1920). Upper left inset indicates 1912 earthquake location relative to 1939–1999 earthquake sequence. Lower right inset shows isoseismals (dashed lines) of 9 August earthquake (EQ) and Marmara seismic gap (Ambraseys and Finkel, 1987).

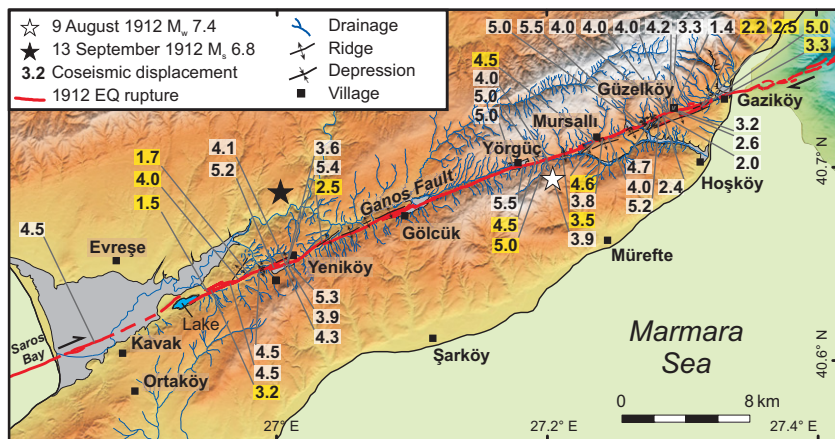


Figure 2. Ganos fault onshore and A.D. 1912 coseismic slip distribution (in meters). Yellow boxes correspond to measures of this study. EQ—earthquake.

The offshore fault zone east of Gaziköy forms a restraining bend (i.e., Tekirdağ bend; $17^\circ \pm 3^\circ$) and can be traced in the Sea of Marmara toward the Central Basin as a nearly east-west–trending continuous rupture (Fig. 1; Okay et al., 2004). In Saros Bay, the on-land Ganos fault extends farther west for an additional minimum 40 km, as shown by clear offshore fault scarps (Ustaömer et al., 2008; McNeill et al., 2004).

1912 EARTHQUAKE SEQUENCE

The 9 August 1912 earthquake occurred along the Ganos fault with an epicenter near Mürefte village (Fig. 1; Ambraseys and Finkel, 1987; Ambraseys and Jackson, 2000). The earthquake was followed by numerous aftershocks, caused severe damage in the Thrace region, and was recorded worldwide at more than 56 instrumental seismic stations (Mihailovic, 1927). Field investigations carried out within a few days and weeks after the mainshock resulted in three key contemporaneous earthquake reports (i.e., Macovei, 1913; Mihailovic, 1927; Sadi, 1912) that provide ample descriptions of surface faulting, landslides, and detailed accounts of damage distribution. Coseismic surface ruptures were visible all along the ~45 km on-land section of the Ganos fault (Fig. 2), and contemporaneous photographs show remarkable mole tracks in fields near Mursallı and Gaziköy (Figs. DR1 and DR2 in the GSA Data Repository¹; Mihailovic, 1927). The maximum damage, localized between Tekirdağ and Mürefte, indicates $I_0 = IX-X$ MSK (maximum intensity in Medvedev-Sponheuer-Karnik scale; Fig. 1; Ambraseys and Finkel, 1987). The earthquake size determined from historical seismic records and field observations yields $M_s = 7.3 \pm 0.3$

(Ambraseys and Jackson, 2000) and M_w 7.4 (Altunel et al., 2004), respectively. Since the 1912 Mürefte earthquake and the 1999 Izmit earthquake have essentially the same size (i.e., M_w 7.4), one may assume that both events have a comparable rupture length (120 ± 20 km). Taking into account the 45-km-long surface rupture onshore, ~75 km rupture should be offshore.

A second large event, recorded in at least 17 worldwide seismic stations, occurred on 13 September 1912 (Fig. 1; $I_0 = VII$ MSK, Hecker, 1920; M_s 6.8 ± 0.35 , Ambraseys and Jackson, 2000). Using a regional bilinear relation, Ambraseys and Jackson (2000) estimated a 2.19×10^{19} Nm seismic moment (M_w 6.8) and suggested a 37-km-long coseismic rupture for this large second shock. Contemporary and recent analyses of seismic records locate the event around Saros Bay, west of the first shock (Walker, 1912; Mihailovic, 1927; Ambraseys and Jackson, 2000). The shock caused further damage with new landslides along the Gelibolu peninsula and Ganos region. In addition, widespread liquefaction occurred in the Saros region (Hecker, 1920; Ambraseys and Finkel, 1987). The damage and size of the event, significant enough to rupture the entire seismogenic zone, suggest that the 13 September earthquake is most likely the southwest continuation of the 9 August rupture rather than a large aftershock.

In order to study the 9 August mainshock, we collected 73 historical seismic records that also include the 13 September 1912 earthquake (e.g., Fig. 3A; Fig. DR3); in the case of historical seismograms it is useful to have access to the record of a similar but a relatively smaller earthquake from the same station to eliminate the influence of unknown parameters. This is the base of the empirical Green function (EGF) approach, first proposed by Hartzell (1978) and further developed in the past 30 yr (e.g., Velasco et al., 1994; Vallée, 2004). The EGF method involves the deconvolution of the smaller earth-

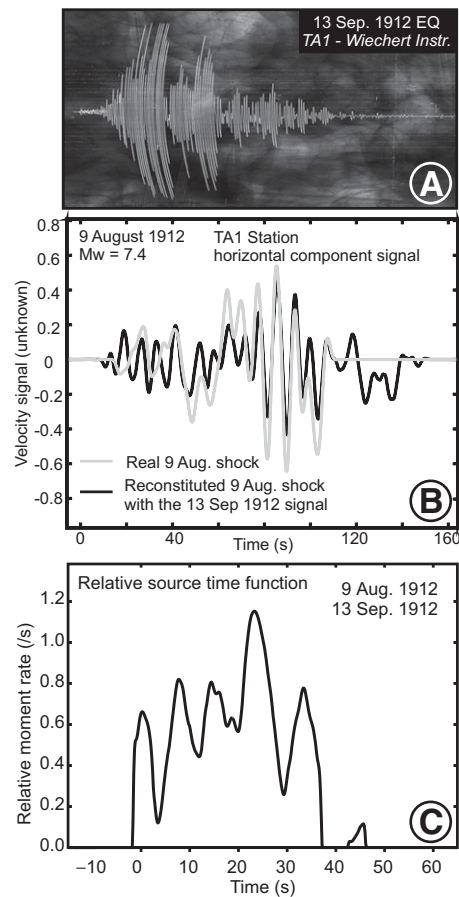


Figure 3. A: Historical seismic record collected and digitized for this study. B: Digitized seismogram of Taranto station (Italy) and waveform modeling showing comparison between real (gray) and reconstituted (black) 9 August 1912 shock. C: Relative source time function of 9 August 1912 and 13 September 1912 earthquakes gives ratio of 0.9–1 in moment magnitude and ~40 s rupture duration.

quake waveform from the large one, giving a good estimate of the source time function of the larger earthquake. We digitized seismograms of both shocks to study seismic source properties and used the deconvolutive approach proposed by Vallée (2004). The mainshock body waves’ deconvolution from the smaller 13 September event (Fig. 3B) at Taranto station (TA1, Italy) provides the relative source time function shown in Figure 3C. Inspection of this source time function shows that the wave emission lasted 40 s; this may correspond to the source duration of the 9 August event. The relative source time function also indicates that the moment ratio between the 9 August and 13 September shocks is ~30, which corresponds to a factor of 0.9–1 difference in magnitude (Fig. 3C). Although limited by the results on a single seismic station (TA1), the duration implies a minimum 110 ± 30 km coseismic rupture length at 2–3.5 km/s rupture propagation; here

¹GSA Data Repository item 2010276, appendix, Table DR1, and Figures DR1–DR4, is available online at www.geosociety.org/pubs/ft2010.htm, or on request from editing@geosociety.org or Documents Secretary, GSA, P.O. Box 9140, Boulder, CO 80301, USA.

we disregard supershear velocities and bilateral propagation as observed during the 1999 Izmit earthquake along straight fault section similar to the Ganos fault (Bouchon et al., 2002). Although most seismograms are for north-south and east-west components, P-wave polarities at 5 stations (Fig. 1) and a field-based N68°E fault strike show a strike-slip mechanism (Fig. 1).

The size of the 9 August shock ($M_s = 7.3 \pm 0.3$; Ambraseys and Jackson, 2000) corresponds to $M_o = 1.23 \cdot 10^{20}$ N m using the Ekström and Dziewonski relation (1988). Assuming 2.0–3.0 m average slip and 15–18 km fault width, the seismic moment implies a 130 ± 15 rupture length, in agreement with the wave form analysis.

FAULT GEOMETRY AND COSEISMIC SLIP DISTRIBUTION

The 1912 on-land rupture is clearly visible along strike due to pressure ridges, sag-ponds, stepovers, shutter ridges, and coseismic right-lateral offsets (<6 m; Figs. 2 and 4A). The surface rupture and coseismic slip illustrate fault discontinuities at depth that may cause stress concentrations significant enough to arrest rupture propagation (Wesnously, 2006).

The N68°E trending on-land rupture shows three 20–30-km-long geometrical segments separated by two releasing basins (<1 km in width; Figs. 2 and 4A). Typical strike-slip rupture morphologies associated with Riedel shears are illustrated in historical documents (Mihailovic, 1927) at sites where we observe 3–5 m right-lateral slip near Gaziköy and Mursallı village (Figs. DR1 and DR2).

Ambraseys and Finkel (1987) suggested a maximum 3 m of right-lateral slip for the 9 August 1912 Mürefte earthquake. The previously reported offsets of Altunel et al. (2004)

are not evenly distributed along strike and form gaps at the two tips of the inland section. Our study raises the number of slip measurements from 31 to 45 offsets, and fills the gaps along the fault (Figs. 2 and 4). The right-lateral displacements range from 1.4 to 5.5 m, most being >3 m, since only large offsets are preserved today. Many offsets larger than 4 m (maximum 5.5 m) are measured along the Güzelköy subsegment and 5–5.4 m right-lateral slip is measured on the eastern tip of the Yeniköy subsegment (Fig. 4). On the Saros subsegment, Rockwell et al. (2009) estimated a 4.5 m right-lateral offset related to the 1912 earthquake. Considering the lack of minimum offsets, the overall slip distribution indicates an average of 2.5 m with 4.5 and 5 m offsets at the western and eastern fault tips of Saros and Gaziköy, respectively. This implies that the 1912 rupture continued offshore into Saros Bay and the Sea of Marmara.

The offshore fault scarp mapped by Armijo et al. (2005) in the Sea of Marmara and by Ustaömer et al. (2008) in Saros Bay suggests the existence of submarine geometrical segments (Fig. 4). A significant restraining bend (17°) is observed between the on-land linear strike-slip fault and the N88°E trending 65 km offshore fault from Gaziköy to the Central Basin (Figs. 1 and 4). Here, a displaced ridge along the Western High subsegment displays 6 ± 1 m of right-lateral slip, presumably due to the 1912 earthquake (Armijo et al., 2005; Fig. 4), but it may also include the penultimate event. Ustaömer et al. (2008) documented a N68°E trending impressive fresh fault scarp in Saros Bay that affects the Saros shelf and the Saros Basin (Fig. 1), where we note the existence of clear cumulative right-lateral offset (that likely includes the 1912 faulting event) visible on

ridges and stream channels. The linear fault geometry in the shelf is followed farther west by a complex dissected fault system within a 5-km-wide half-graben structure (Saros Basin; Fig. 1; Ustaömer et al., 2008; McNeill et al., 2004). The 1912 surface rupture, slip distribution, and complex fault geometry both on land and offshore depict a discontinuous fault geometry at depth, where the 7-km-wide Central pull-apart basin, the Ganos 17° bend, and the 5-km-wide Saros half graben basin may act as major obstacles to the rupture propagation.

DISCUSSION AND CONCLUSIONS

Our recent field investigations of the 1912 Ganos fault segment document the on-land rupture geometry and related segmentation with slip distribution (Figs. 1 and 2). A maximum 5.5 m of right-lateral slip is measured on land along the Ganos fault, from which we infer an average 2.5 m of slip, comparable to the 1999 Izmit earthquake (Barka et al., 2002). We provide a strike-slip focal mechanism for the first mainshock from P-wave arrivals. Using seismic records of the 9 August and 13 September shocks from the Italian TA1 station, we performed a deconvolution modeling and obtained an ~40 s source duration for the first shock. Field measurements of coseismic slip and fault segmentation and estimated 120 ± 30 km long fault rupture are consistent with the inferred rupture duration (Figs. 1 and 3B) and the earthquake size (M_w 7.4). Together, this confirms that a significant portion of the earthquake rupture is offshore and, assuming ~30 km rupture length for the second shock, the total earthquake fault rupture length sums to 150 ± 30 km.

The analysis of the onshore and offshore fault geometry indicates that the only major barriers to

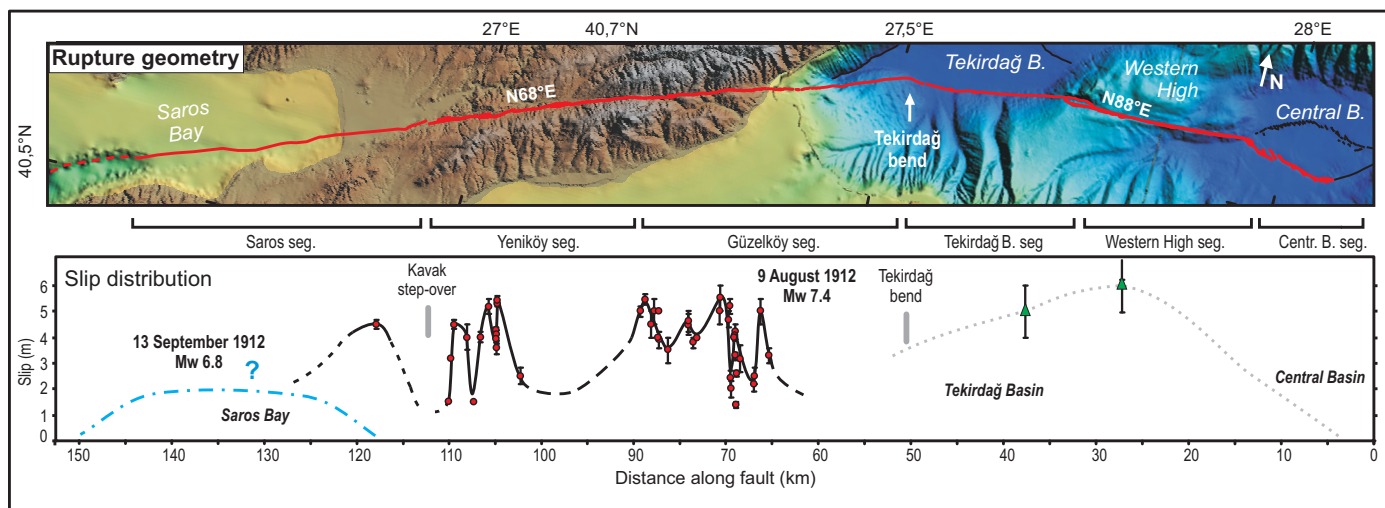


Figure 4. Ganos fault segment (seg.) and A.D. 1912 coseismic slip distribution. Subsegments along fault zone indicate geometrical complexities. The 150-km-long fault (red lines in upper panel) includes 9 August and 13 September earthquake ruptures. Marmara Sea slip values (two triangles in lower panel; Armijo et al., 2005) and inferred dashed line may include penultimate earthquake. Blue dashed line is estimated slip distribution ($\bar{U} = 1.2$ m) for Mw 6.8 strike-slip earthquake. B.—Basin (Central).

the earthquake rupture propagation are the Saros and Central pull-apart basins (cf. Wesnousky, 2006). These barriers are comparable to the Çınarcık and Düzce basins that stopped the 1999 Izmit earthquake rupture propagation (Barka et al., 2002). If, as suggested by Le Pichon et al. (2003) and Altınok et al. (2003), the 9 August rupture stops at the Tekirdağ restraining bend, the 120 ± 30 km rupture length determined from field observations, seismic moment, and source time function requires that the 13 September earthquake epicenter be located far west, beyond the Dardanelles. However, such a scenario fails to explain the damage distribution given by Hecker (1920) and the epicentral location estimated by Ambraseys and Finkel (1987). In addition, it overlaps the epicenter region of the well-defined 27 March 1975 $M_w = 6.6$ earthquake, which most likely ruptured a significant portion of the fault in Saros Bay (Fig. 1, Ambraseys and Jackson, 2000). Therefore, the 9 August rupture must have propagated mostly into the Sea of Marmara rather than toward Saros Bay, and, having crossed the restraining bend, necessarily reached the Central Basin, in agreement with the Armijo et al. (2005) study. The 150 ± 30 km total rupture length includes (1) the three segments in the Sea of Marmara (~65 km) beginning from the Central Basin, (2) the on-land fault section (~45 km), and (3) the Saros Bay segment (~40 km) limited by the Saros pull-apart basin. The eastern termination of the 9 August 1912 rupture and the western termination of the 1999 earthquake rupture (Çakır et al., 2003) imply a minimum 100-km-long seismic gap in the Sea of Marmara. This fault length suggests an earthquake size, $M > 7$, that should be taken into account in any seismic hazard assessment of the Istanbul region.

ACKNOWLEDGMENTS

This work was supported by the RELIEF (Reliable Information on Earthquake Faulting) project (European Commission contract EVG1-2002-00069). Aksoy benefited from a Ph.D. fellowship from the French Embassy in Ankara. We thank Matthieu Ferry, Rob Langridge, and Ahmet Akoğlu for their comments on the manuscript, Hayrullah Karabulut (Kandilli Observatory, Istanbul), and Michel Bouchon (Laboratoire de Géophysique Interne et Tectonophysique, Grenoble) for fruitful discussions, and Antoine Schlupp (Institut de Physique du Globe de Strasbourg) for his support in digitizing seismic records. We are grateful to Josep Batllo (Instituto Dom Luiz, Lisbon), and Graziano Ferrari (Istituto Nazionale di Geofisica e Vulcanologia, Bologna) for the access to the SISMOS database and to seismological centers for sending us seismic records.

REFERENCES CITED

Altınok, Y., Alpar, B., and Yalıtırak, C., 2003, Şarköy-Mürefte 1912 earthquake's tsunami, extension

of the associated faulting in the Marmara Sea, Turkey: *Journal of Seismology*, v. 7, p. 329–346, doi: 10.1023/A:1024581022222.

Altunel, E., Meghraoui, M., Akyüz, H.S., and Dikbaş, A., 2004, Characteristics of the 1912 co-seismic rupture along the North Anatolian fault zone (Turkey): Implications for the expected Marmara earthquake: *Terra Nova*, v. 16, p. 198–204, doi: 10.1111/j.1365-3121.2004.00552.x.

Ambraseys, N.N., and Finkel, C.F., 1987, The Saros-Marmara earthquake of 9 August 1912: *Earthquake Engineering & Structural Dynamics*, v. 15, p. 189–211, doi: 10.1002/eqe.4290150204.

Ambraseys, N.N., and Jackson, J.A., 2000, Seismicity of the Sea of Marmara (Turkey) since 1500: *Geophysical Journal International*, v. 141, no. 3, p. F1–F6.

Armijo, R., and 22 others, 2005, Submarine fault scarps in the Sea of Marmara pull-apart (North Anatolian fault): Implications for seismic hazard in Istanbul: *Geochemistry Geophysics Geosystems*, v. 6, Q06009, 29 p., doi: 10.1029/2004GC000896.

Barka, A., and 21 others, 2002, The surface rupture and slip distribution of the 17 August 1999 Izmit earthquake (M 7.4): North Anatolian fault: *Seismological Society of America Bulletin*, v. 92, no. 1, p. 43–60, doi: 10.1785/0120000841.

Barka, A.A., and Kadinsky-Cade, K., 1988, Strike-slip fault geometry in Turkey and its influence on earthquake activity: *Tectonics*, v. 7, p. 663–684, doi: 10.1029/TC007i003p00663.

Bouchon, M., Töksöz, M.N., Karabulut, H., Bouin, M.P., Dietrich, M., Aktar, M., and Edie, M., 2002, Space and time evolution of rupture and faulting during the 1999 Izmit (Turkey) earthquake: *Seismological Society of America Bulletin*, v. 92, no. 1, p. 256–266, doi: 10.1785/0120000845.

Çakır, Z., de Chabalière, J.-B., Armijo, R., Meyer, B., Barka, A., and Peltzer, G., 2003, Coseismic and early postseismic slip associated with the 1999 Izmit earthquake (Turkey), from SAR interferometry and tectonic field observations: *Geophysical Journal International*, v. 155, p. 93–110, doi: 10.1046/j.1365-246X.2003.02001.x.

Ekström, G., and Dziewonski, A.M., 1988, Evidence of bias in estimations of earthquake size: *Nature*, v. 332, p. 319–323, doi: 10.1038/332319a0.

Hartzell, S., 1978, Earthquake aftershocks as Green's functions: *Geophysical Research Letters*, v. 5, p. 1–4, doi: 10.1029/GL005i001p00001.

Hecker, O., 1920, Mitteilungen über Erdbeben im Jahre 1912: Jena, A. Sieberg, Hauptstation für Erdbebenforschung, 26 p.

Hubert-Ferrari, A., Barka, A.A., Jacques, E., Nalbant, S.S., Meyer, B., Armijo, R., Taponnier, P., and King, G.C., 2000, Seismic hazard in the Marmara Sea region following the 17 August 1999 Izmit earthquake: *Nature*, v. 404, p. 269–273, doi: 10.1038/35005054.

Karabulut, H., Roumelioti, Z., Benetatos, C., Ahu Komec, M., Özalaybey, S., Aktar, M., and Kiratzi, A., 2006, A source study of the 6 July 2003 (M_w 5.7) earthquake sequence in the Gulf of Saros (northern Aegean Sea): *Seismological evidence for the western continuation of the Ganos fault: Tectonophysics*, v. 412, p. 195–216, doi: 10.1016/j.tecto.2005.09.009.

Le Pichon, X.L., Chamot-Rooke, N., Rangin, C., and Şengör, C., 2003, The North Anatolian fault in

the Sea of Marmara: *Journal of Geophysical Research*, v. 108, doi: 10.1029/2002JB001862.

Macovei, G., 1913, *Aspura Cutremurului de Pamant dela Mare de Marmara dela 9 August 1912*: Academia Romana, Publicatiunile Adamachi, v. 33, p. 260–273.

McNeill, L.C., Mille, A., Minshull, T.A., Bull, J.M., Kenyon, N.H., and Ivanov, M., 2004, Extension of the North Anatolian fault into the North Aegean Trough: Evidence for transtension, strain partitioning, and analogues for Sea of Marmara basin models: *Tectonics*, v. 23, TC2016, 12 p., doi: 10.1029/2002TC001490.

Mihailovic, J., 1927, Trusne katastrofe na Mramornome moru, in *Posebno izdanje srpske akademije nauka Volume 65*: Belgrad, Srpske Kraljevske Akademije, p. 1–303.

Okay, A.I., Tüysüz, O., and Kaya, S., 2004, From transpression to transtension: Changes in morphology and structure around a bend on the North Anatolian fault in the Marmara region: *Tectonophysics*, v. 391, p. 259–282, doi: 10.1016/j.tecto.2004.07.016.

Rockwell, T., and 12 others, 2009, Palaeoseismology of the North Anatolian fault near the Marmara Sea: Implications for fault segmentation and seismic hazard, in Reichert, K., et al., eds., *Palaeoseismology: Historical and prehistorical records of earthquake ground effects for seismic hazard assessment*: Geological Society of London Special Publication 316, p. 31–54, doi: 10.1144/SP316.3.

Sadi, D.Y., 1912, *Marmara Havzasının 26–27 Temmuz Hareket-i Arzı 15 Eylül 1328*: İstanbul, Resimli Kitap Matbaası, p. 45.

Ustaömer, T., Gökaşan, E., Tur, H., Görüm, T., Batuk, F., Kalafat, D., Alp, H., Ecevitoglu, B., and Birkan, H., 2008, Faulting, mass-wasting and deposition in an active dextral shear zone, the Gulf of Saros and the NE Aegean Sea, NW Turkey: *Geo-Marine Letters*, v. 28, no. 3, p. 171–193, doi: 10.1007/s00367-007-0099-6.

Vallée, M., 2004, Stabilizing the empirical Green function analysis: Development of the projected Landweber method: *Seismological Society of America Bulletin*, v. 94, no. 2, p. 394–409, doi: 10.1785/0120030017.

Velasco, A.A., Ammon, C.J., and Lay, T., 1994, Empirical Green function deconvolution of broadband surface waves: Rupture directivity of the 1992 Landers, California ($M_w = 7.3$), earthquake: *Seismological Society of America Bulletin*, v. 84, p. 735–750.

Walker, W.G., 1912, Turkish earthquake of September 13: *Nature*, v. 90, p. 163, doi: 10.1038/090163d0.

Wesnousky, S.G., 2006, Predicting the endpoints of earthquake ruptures: *Nature*, v. 444, no. 7117, p. 358–360, doi: 10.1038/nature05275.

Manuscript received 6 June 2010

Revised manuscript received 14 June 2010

Manuscript accepted 15 June 2010

Printed in USA